INSTITUTE OF PHYSICS PUBLISHING JOURNAL OF PHYSICS D: APPLIED PHYSICS

J. Phys. D: Appl. Phys. **38** (2005) 2135–2141 doi:10.1088/0022-3727/38/13/009

High-performance mid-infrared quantum dot infrared photodetectors

S Chakrabarti[1], A D Stiff-Roberts[1,3], X H Su[1], P Bhattacharya[1], G Ariyawansa[2] and A G U Perera[2]

[1] Solid State Electronics Laboratory, Department of Electrical Engineering and Computer Science, University of Michigan, Ann Arbor, MI 48109-2122, USA
[2] Department of Physics and Astronomy, Georgia State University, Atlanta, GA 30303, USA

Received 21 December 2004, in final form 23 February 2005
Published 17 June 2005
Online at stacks.iop.org/JPhysD/38/2135

Abstract

Quantum dot infrared photodetectors (QDIPs) have emerged as attractive devices for sensing long wavelength radiation. Their principle of operation is based on intersublevel transitions in quantum dots (QDs). Three-dimensional quantum confinement offers the advantages of normal incidence operation, low dark currents and high-temperature operation. The performance characteristics of mid-infrared devices with three kinds of novel heterostructures in the active region are described here. These are a device with upto 70 QD layers, a device with a superlattice in the active region, and a tunnel QDIP. Low dark currents (1.59 A cm^{-2} at 300 K), large responsivity (2.5 A W^{-1} at 78 K) and large specific detectivity (10^{11} cm Hz$^{1/2}$ W^{-1} at 100 K) are measured in these devices. It is evident that QDIPs will find application in the design of high-temperature focal plane arrays. Imaging with small QD detector arrays using the raster scanning technique is also demonstrated.

(Some figures in this article are in colour only in the electronic version)

1. Introduction

Quantum dot infrared photodetectors (QDIPs), consisting of self-organized In(Ga)As/Ga(Al)As quantum dot (QD) active regions, have emerged as a technology capable of detecting light across a broad range of infrared (IR) wavelengths [1–7]. Compared to more conventional quantum-well infrared photodetectors (QWIPs), the advantages of QDIPs result from three-dimensional carrier confinement in QDs. The associated advantages include: (i) intrinsic sensitivity to normal-incidence light, (ii) longer lifetime of photo-excited electrons due to reduced electron–phonon scattering and (iii) lower dark current which can lead to high-temperature operation (>120 K).

Despite these advantages, the demonstration of large responsivity in QDIPs has been elusive due to the identical transport paths that exist for photocurrents and dark currents. Therefore, heterostructure designs developed to minimize the dark current, such as the insertion of a single AlGaAs barrier outside the active region, also prevent the efficient collection of carriers contributing to the photocurrent, resulting in low responsivity values (∼1 mA W^{-1}) [7]. In addition, while the calculated absorption coefficient for a single layer of In(Ga)As/GaAs QDs is large, the quantum efficiency of QDIPs tends to be low for several reasons. First, in the surface-normal direction, the absorption region is very thin since QDIPs typically have 10–20 layers of QDs. Second, the typical In(Ga)As/GaAs QD surface density is $\sim 5 \times 10^{10}$ cm^{-2}, and the corresponding fill factor ranges from 25% to 28%. Therefore, the IR absorption (and quantum efficiency) of QDIPs can be improved by increasing the active region volume in these devices, leading to higher responsivity. Furthermore, the ability to reduce the dark current, without reducing the photocurrent, might enhance the performance characteristics of QDIPs in terms of responsivity, detectivity and the temperature of operation.

In this paper, we present three advanced heterostructure designs for obtaining improved responsivity in In(Ga)As/Ga(Al)As mid-infrared (mid-IR) QDIPs. In the first, the absorption volume is increased by introducing a large number of QD layers in the active region. By controlling the barrier width between the dot layers, 70 layers of InAs/GaAs

[3] Present address: Department of Electrical and Computer Engineering, Duke University, 3511 CIEMAS, Box 90291, Durham, NC 27708-0291, USA.

QDs were grown with a minimal amount of dislocation generation. The large GaAs barriers also help to reduce the dark current in these devices. In the second device, InAs QDs were grown directly on the AlAs layer of a GaAs/AlAs superlattice (SL) with a 15 nm period. Due to the reduced mobility of Al compared to In, the dot density increased as a result of the altered adatom kinetics [8, 9]. The large dot density permits increased absorption of IR light. This device heterostructure, featuring a GaAs/AlAs SL barrier, is a modification of the dot-in-a-well (DWELL) structure [10, 11], and it benefits from several advantages, including: (i) increased carrier confinement due to the AlAs barriers, (ii) spectral response tunability due to several transitions that can occur between the QDs and the SL minibands and (iii) efficient transport of the photo-excited carriers to the device contacts. In the third device, we have incorporated a double barrier resonant tunnelling AlGaAs/GaAs heterostructure with each In(Ga)As/GaAs QD layer, so as to suppress the dark current while allowing the photocurrent, corresponding to the design wavelength to be transmitted [12]. The obvious advantage is that we can selectively tune the peak wavelength of photo-response, while blocking the broad distribution of carriers contributing to the dark current. On account of the extremely low dark currents expected in these devices, higher temperature of operation and enhanced detectivity are expected. The ultimate objective is to get high-temperature (>150 K) QD focal plane arrays (FPAs) for imaging purposes.

The design and fabrication of a fully operational, large-area FPA is both expensive and time-consuming, due in large part to the silicon read-out circuit (Si-ROIC) that must be hybrid bump-bonded (or flip-chip bonded) to the detector array. Such a read-out circuit allows for independent access to each pixel in the detector array for digital signal processing of an image. In an effort to demonstrate imaging with QDIPs in a less rigorous manner, we have developed a raster-scan imaging system in which the field-of-view is scanned simultaneously in the x- and y-axes by a raster scan motion provided by two mirrors. An array of photocurrent/voltage values is compiled as the field-of-view array elements are scanned either by a single detector or a small interconnected detector array. In the following sections, we report the growth, fabrication and characterization of the three different QDIP heterostructure designs for large responsivity along with some results of raster-scan imaging using small QDIP arrays.

2. Device growth and fabrication

In order to increase IR absorption, we have studied the molecular beam epitaxial (MBE) growth and material characteristics of large QD stacks using transmission electron microscopy (TEM) images. We have grown a 70 layer QDIP heterostructure on a semi-insulating (100) GaAs substrate, schematically shown in figure 1(*a*). The conduction band profile under bias is also shown in this figure. A 5000 Å bottom GaAs contact layer ($n = 2\times10^{18}$ cm^{-3}) and a 2000 Å top GaAs contact layer ($n = 2 \times 10^{18}$ cm^{-3}) were included. A 500 Å GaAs intrinsic buffer was grown at 620°C after the bottom contact layer and before the first QD layer. The InAs QDs were 2.0 monolayers (MLs) thick and doped with Si to a nominal concentration of $n = 1 \times 10^{18}$ cm^{-3}. A 400 Å $Al_{0.3}Ga_{0.7}As$

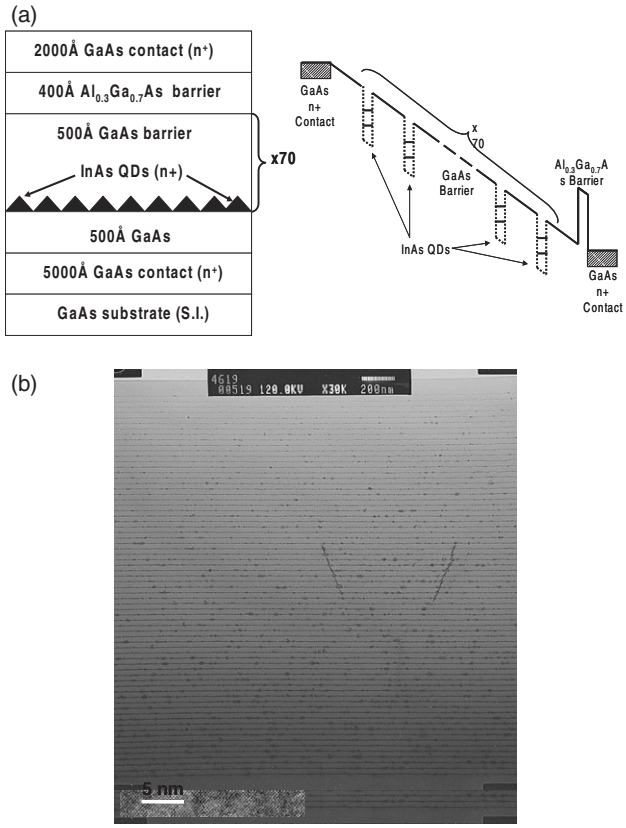

Figure 1. (*a*) Schematic of the 70 layer InAs/GaAs QDIP heterostructure and conduction band profile under bias; (*b*) transmission electron microscopy image of 70 layer InAs/GaAs QD stack showing that very few dislocations are propagated throughout the heterostructure.

current-blocking barrier was grown after the last GaAs barrier and before the top GaAs contact layer. An important aspect of the MBE growth procedure used to obtain these large QD stacks is the substrate temperature cycling that takes place during the growth of the GaAs barrier. The most important parameter that had to be optimized, to increase the number of QD layers without generating dislocations, was the GaAs barrier width. The TEM image of 70-dot layers with an optimized GaAs barrier width of 500 Å, is shown in figure 1(*b*). The usual size variation was observed in the QD heterostructure, with larger dots located at the top of the QD stack and smaller dots located near the bottom of the stack.

A schematic of the heterostructure for the second device, the SL DWELL QDIP, along with the band diagram for the active region under bias, is shown in figure 2(*a*). This device was grown on an n^+ GaAs (001) substrate. After growth of a 100 nm Si doped contact layer, a 1 nm thick AlAs layer was deposited. The InAs QDs were formed by depositing ∼2 MLs of InAs (at a rate of 0.1 ML s^{-1}) on the AlAs layer. A one minute pause followed, in order to allow complete formation of the QDs. This was followed by a 14 nm GaAs cap layer over the QDs. The ∼15 nm thick heterostructure, consisting of the AlAs layer, the InAs QDs and the GaAs cap layer, was repeated 10 times. Finally, 200 nm of Si doped GaAs was deposited to form the top contact layer. Except for the initial GaAs contact layer, which was grown at 600°C, all the other layers were grown at 490°C. Surface atomic force microscopy (AFM)

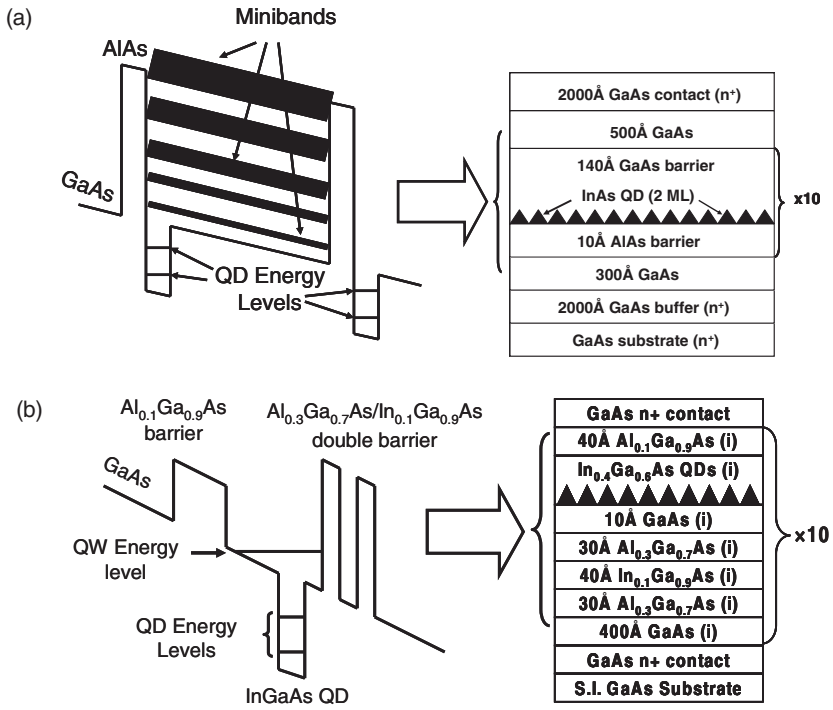

Figure 2. (*a*) Schematic of the conduction band of the SL QDIP, demonstrating the formation of minibands, along with the heterostructure schematic; (*b*) conduction band profile of the T-QDIP under an applied transverse bias along with the schematic of the T-QDIP heterostructure.

images on dot layers grown on AlAs under similar growth conditions show a dot density of $\sim 10^{12}$ cm^{-2}; therefore, this growth technique significantly increases the efficiency with which IR light can be absorbed.

The tunnelling QDIP (T-QDIP) device heterostructure, grown on a (001)-oriented semi-insulating GaAs substrate, is schematically shown in figure 2(*b*), along with the conduction band profile of one period in the active region, under bias. The GaAs and AlGaAs layers were grown at 610°C and the QDs were grown at 500°C. Before initiating the growth of the QDs, 10 Å of GaAs was grown on the $Al_{0.3}Ga_{0.7}As$ barrier of the resonant tunnelling heterostructure, to smoothen out the growing surface. This was followed by the deposition of six MLs of InGaAs to form the self-organized QDs. A $Al_{0.1}Ga_{0.9}As$ barrier of thickness 30 Å is incorporated on the other side of the dot, opposite to the double barrier. As shown, the 10-dot layers with accompanying double barrier structures were grown, separated by 400 Å GaAs barrier layers. Growth is terminated with a 0.2 μm silicon-doped ($n = 2 \times 10^{18}$ cm^{-3}) GaAs top contact layer.

Devices for all three types of QDIPs described above were fabricated by a three-step process consisting of standard photolithography and wet-etch techniques: (1) evaporation of the top metal ring contact; (2) wet chemical etching to define the circular mesa active region and (3) evaporation of the bottom metal ring contact. Detectors with radii ranging from 100 to 300 μm were then annealed at 400°C for one minute to obtain ohmic contacts.

For the array, the InAs/GaAs QDIP heterostructure used is similar to that in figure 1(*a*), except for having ten layers of 2.2 ML InAs QDs, surrounded by 250 Å GaAs barriers. While raster-scan imaging should work with a single detector, a small array was actually used because it is easier to collect infrared light over a larger area. Standard photolithography and wet-etch processing were used to fabricate (13 × 13) non-addressable (interconnected) arrays of vertical, mesa-shaped QDIPs. The pixel diameter was 40 μm, and the array pitch was 120 μm.

3. Detector characteristics, results and discussions

3.1. Measurement techniques

In order to conduct measurements, the devices are glued on chip carriers with silver paint and individual devices are wire bonded to separate leads of the carriers. The chip carriers are then mounted into a liquid helium cryostat. Several measurements have been conducted in order to characterize the QDIP, namely: (1) dark current; (2) spectral response; (3) noise spectra and specific detectivity (D^*) and (4) photoconductive gain.

3.1.1. Dark current measurements. Dark-current–voltage (I–V) characteristics are measured with a Hewlett-Packard 4145 Semiconductor Parameter Analyser at several temperatures in the range 78–300 K. Measurements are made for both bias polarities, where a positive bias corresponds to positive polarity of the top contact layer.

3.1.2. Spectral response and responsivity measurements. The spectral response and responsivity were measured for normal incidence using a globar broadband source, a composite bolometer with a known sensitivity, and a Perkin-Elmer S2000 Fourier transform infrared spectrometer.

Both the test QDIP and the bolometer spectra are measured concurrently with the same combination of optical elements, so that the optical path is identical. The voltage responsivity is expressed as

$$R\left(\frac{V}{W}\right) = \frac{G I_{\mathrm{d}} S_0}{I_{\mathrm{b}}}, \tag{1}$$

where I_{d} is the device spectrum, I_{b} the bolometer spectrum, S_0 the bolometer sensitivity and G a geometrical factor that corrects for differences in the radiation-incident-area of the detector and the bolometer. The current responsivity is obtained by dividing the voltage responsivity by the effective resistance R_{e}. The detector and the load resistor are parallelly connected, which yields $R_{\mathrm{e}} = R_{\mathrm{l}} R_{\mathrm{d}}/(R_{\mathrm{l}} + R_{\mathrm{d}})$, where R_{l} is the resistance of the load resistor and R_{d} the detector dynamic resistance. The final current responsivity is given by

$$R\left(\frac{A}{W}\right) = \frac{G I_{\mathrm{d}} S_0 (R_{\mathrm{l}} + R_{\mathrm{d}})}{(R_{\mathrm{l}} R_{\mathrm{d}} I_{\mathrm{b}})}. \tag{2}$$

The peak responsivity, R_{peak}, as a function of bias is also determined by measuring the photocurrent I_{photo} with a current amplifier and fast fourier transform (FFT) signal analyser, as the device is irradiated with a 800 K blackbody source. Thus,

$$R_{\mathrm{peak}} = \Gamma \times \frac{I_{\mathrm{photo}}}{P_{\mathrm{incident}}}, \tag{3}$$

where P_{incident} is the photon power impinging on the detector, determined from the blackbody calibration and Γ is a blackbody-to-peak conversion factor, which is inversely proportional to the relative response (per watt) measured by the FTIR spectral response.

3.1.3. Noise spectra and specific detectivity. The specific detectivity, which is a measure of the signal-to-noise ratio of the device, was obtained from the measured peak responsivity R_{p} and noise density spectra S_{i} at different temperatures and applied biases. The noise spectra were measured with a dual channel FFT signal analyser and a low noise pre-amplifier. A thick copper plate was used as a radiation block to provide the dark conditions for the measurements. D^* is calculated by

$$D^* = \frac{R_{\mathrm{p}} A^{1/2}}{S_{\mathrm{i}}^{1/2}} \quad (\mathrm{cm\,Hz^{1/2}\,W^{-1}}), \tag{4}$$

where A is the illuminated area of the detector. A flat-band noise spectrum is desirable because it indicates that the dominant noise mechanism is generation–recombination (GR) noise. However, near zero bias, for frequencies below 500 Hz, the noise is amplifier limited, since the dark current from the QDIP is extremely low. To take into account the amplifier noise, the noise spectrum from the amplifier is subtracted from the signal and noise FFT spectra measured for the QDIP. Another noise contribution at low frequencies is $1/f$ noise, which also prohibits a flat-band noise spectrum. For this, the photocurrent response measurements are obtained by averaging the detector signal over a 50 Hz bandwidth centred around the chopper frequency and averaging the detector noise over a similar bandwidth in a flat-band region (>509 Hz) of the FFT spectrum, taking care to avoid the chopper frequency and multiples of 60 Hz.

3.1.4. Photoconductive gain. The photoconductive gain (g) can be defined as the ratio of total collected carriers to total excited carriers, both thermally generated and photo-generated. Since QDIPs are unipolar devices, the gain may be greater than one if the carrier lifetime exceeds the carrier transit time through the device:

$$g = \frac{\tau_{\mathrm{eff}}}{\tau_{\mathrm{tr}}}, \tag{5}$$

where τ_{eff} is the effective electron lifetime and τ_{tr} is the transit time for an electron to travel across the active region. Experimentally, g is obtained from the relation [7]

$$g = \frac{S_{\mathrm{i}}}{4q I_{\mathrm{dark}}} + \frac{1}{2N}, \tag{6}$$

where I_{dark} is the measured dark current and N is the number of QD layers. However, in the derivation of equation (6), we assume the carrier emission and capture processes are generation–recombination; therefore, the measured g is only valid under those conditions [7].

3.2. InAs/GaAs 70-dot layer QDIP

Measurements on this device were made for both positive (the AlGaAs barrier end having positive polarity) and negative biases. The dark current densities in the 70 layer device are very low compared to previous measurements [7], especially at high operating temperatures ($I_{\mathrm{dark}} = 1.83 \times 10^{-2}\,\mathrm{A\,cm^{-2}}$, $T = 175\,\mathrm{K}$, $V_{\mathrm{bias}} = -2.0\,\mathrm{V}$). The spectral response, shown in figure 3(a), peaks at approximately 3.9 μm and was measured at 150 K. We believe this peak originates from electron transitions from the QD ground state to the continuum states. Figure 3(b) shows the peak responsivity as a function of bias at 175 K. The responsivity is asymmetric with respect to positive and negative biases, and the responsivity increases greatly with increasing forward bias as band bending across the absorption region and the $Al_{0.3}Ga_{0.7}As$ barrier allows more photocurrent to be collected at the contacts. In contrast, higher detectivity is measured for a negative bias, for which the dark current is lower. For $V_{\mathrm{bias}} = 2.0\,\mathrm{V}$, the responsivity is $0.12\,\mathrm{A\,W^{-1}}$. The peak detectivity as a function of temperature is shown in figure 3(c). The maximum detectivity is $\sim 10^{11}\,\mathrm{cm\,Hz^{1/2}\,W^{-1}}$ for $V_{\mathrm{bias}} = -2\,\mathrm{V}$ and $T = 100\,\mathrm{K}$, which is a large value for this temperature. It is evident that greatly improved detector performance can be achieved by increasing the number of dot layers.

3.3. Superlattice DWELL QDIP

Figure 4(a) shows the variation in the peak wavelength of response for SL DWELL QDIPs of different SL periods. The inset to figure 4(a) shows the normalized spectral response obtained from a 200 μm diameter device of period 15 nm at $T = 78\,\mathrm{K}$. The peak response occurs at 4.3 μm. By considering the minibands of the QDIP heterostructure, calculated with a self-consistent Schrödinger–Poisson model, the observed response is most likely due to bound-to-miniband transitions from the QD excited state (60 meV below the GaAs conduction band edge) to the third miniband of the GaAs/AlAs SL. Figure 4(b) shows the measured peak

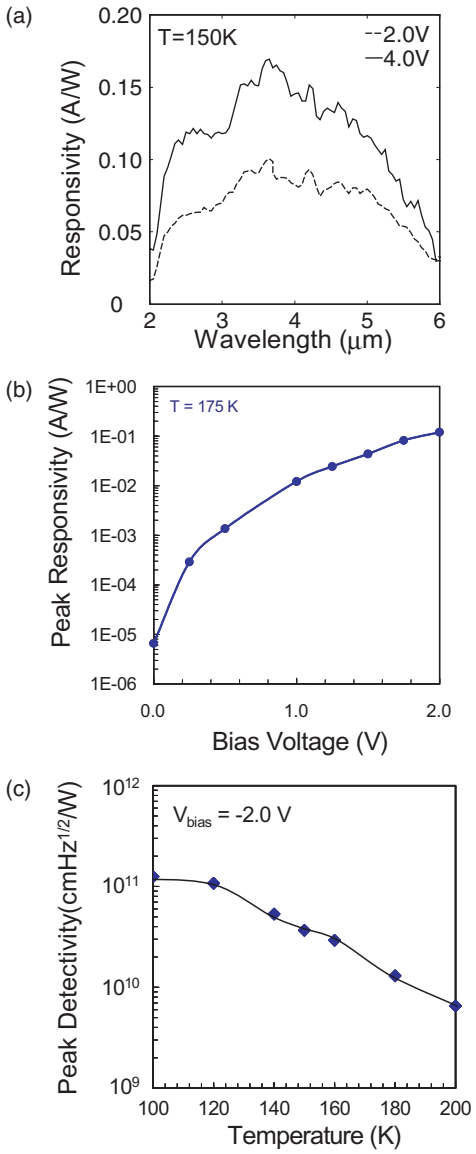

Figure 3. (*a*) Spectral response at $T = 150$ K; (*b*) peak responsivity as a function of bias measured at $T = 175$ K and (*c*) peak detectivity as functions of temperature, for the 70 layer InAs/GaAs QDIP.

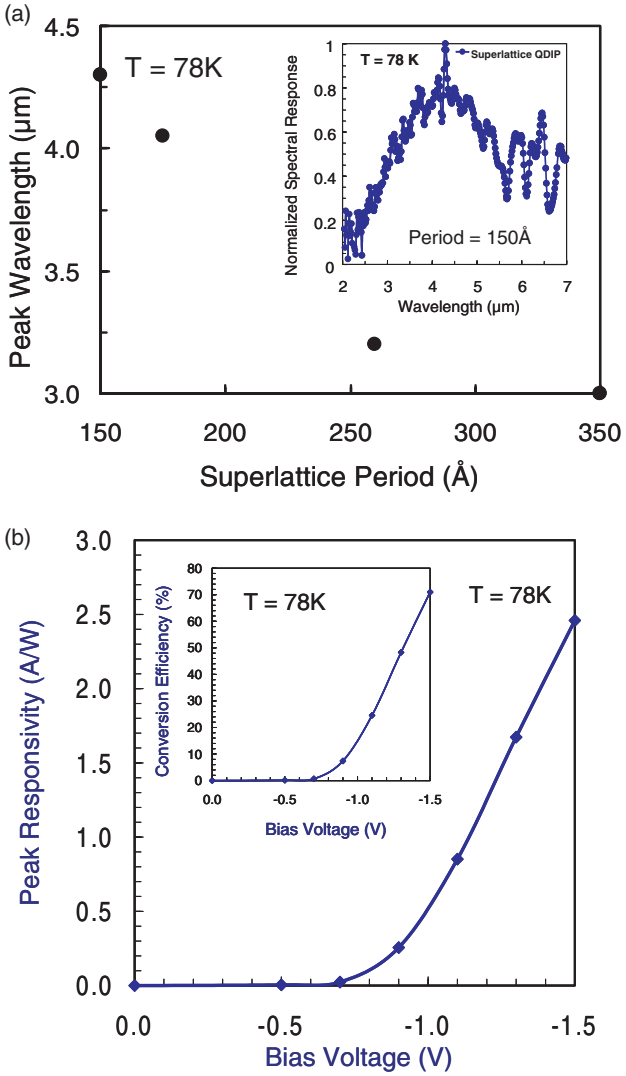

Figure 4. (*a*) Variation of peak wavelength of response for different periods of the SL DWELL QDIPs. The inset shows the normalized spectral response for a 15 nm SL QDIP; (*b*) peak responsivity as functions of bias for the SL DWELL QDIP measured at $T = 78$ K. The inset shows the conversion efficiency as a function of bias at $T = 78$ K.

responsivity as a function of bias. At a detector temperature of 78 K and a bias voltage of −1.5 V, the peak responsivity is 2.5 A W^{-1}. The peak conversion efficiency as a function of bias, shown in the inset of figure 4(*b*), has a maximum value of approximately 70% at the same temperature and bias. The high values of measured responsivity in these devices can be attributed to two factors. First, the density of InAs dots on AlAs is typically an order of magnitude higher than that of dots grown on GaAs. Furthermore, the photoconductive gain in these devices is large (∼5–6), which results from the large electric field across the thin active region. Therefore, the SL DWELL QDIP, which benefits from increased surface density of InAs QDs grown on AlAs, provides state-of-the-art performance in terms of the measured responsivity and conversion efficiency for QDIPs in the mid-wavelength infrared range at 78 K.

3.4. Tunnel QDIP

Figure 5 depicts the measured photoresponse of the tunnel QDIP at high temperatures ($T > 200$ K). There are two distinct absorption peaks, at 6 and 17 μm and these persist even at room temperature. This is possibly due to the extremely low dark current ($J_{\rm dark} = 1.6$ A cm^{-2} at 300 K for 1 V bias). On closer examination, it is apparent that the response centred at 6 μm consists of two closely spaced peaks at 5.7 and 6.2 μm, as shown in the inset of figure 5. The transition wavelength of 6 μm is in excellent agreement with the designed and calculated transition energy of 161 meV for the photo-excited electrons from the ground state in the QD to the quasi-bound state in the well. The peaks at 5.7 and 6.2 μm arise from overlap of the wavefunctions of the quantum well states and the bound states of the double barrier heterostructure. The twin peaks provide experimental evidence of resonant tunnelling in the operation of the device.

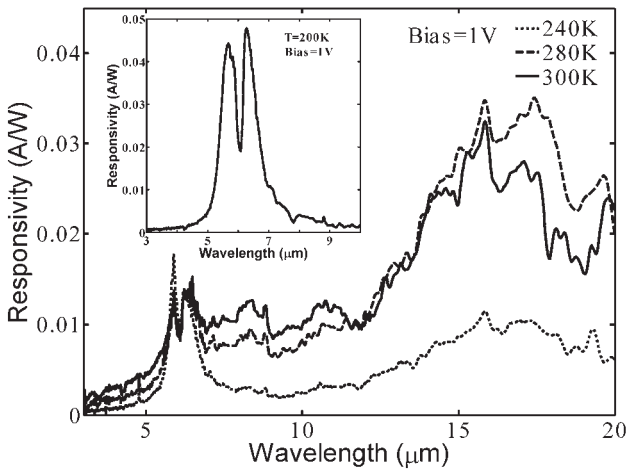

Figure 5. Spectral responsivity of the tunnel QDIP as a function of wavelength at different temperatures. The inset shows spectral responsivity variation for the peak at 6 μm as a function of temperature, illustrating the two closely spaced peaks at 5.7 and 6.2 μm.

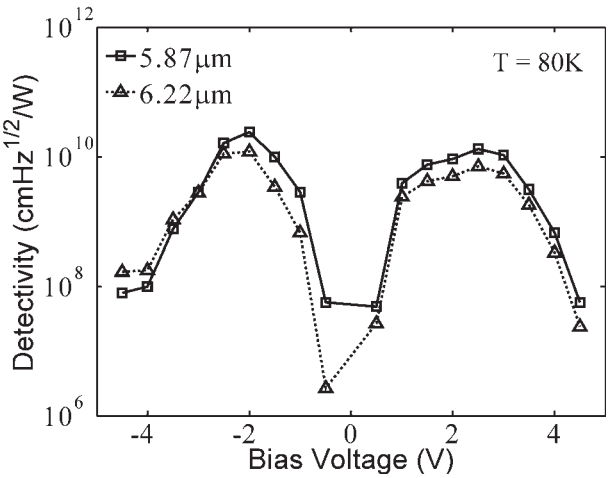

Figure 6. Variation of peak detectivity of the tunnel QDIP as a function of bias at 80 K for the spectral peaks at 5.7 and 6.2 μm, for the T-QDIP.

The estimated value of $\Delta\lambda/\lambda$ for the 5.7 μm peak is 0.3. The peak responsivity is 0.75 A W^{-1} (4 V bias) at 80 K and 0.012 A W^{-1} (1 V bias) at 300 K. The gain of the T-QDIP was determined from noise spectra measurements described in section 3. In the operating bias range of interest, 1–2 V, the gain is found to be unity. The increase in gain beyond 2 V is believed to be due to the onset of avalanche multiplication. Therefore, the responsivity values discussed above reflect the true absorption and photoresponse of the devices. The measured values of D^* at $T = 80$ K are plotted in figure 6 as a function of bias. The value of D^* reaches a maximum value of 2.4×10^{10} cm Hz$^{1/2}$ W^{-1} at -2 V and decreases again due to the monotonic increase of the dark current with bias. For the 17 μm response we measure a peak responsivity of 0.16 A W^{-1} and $D^* = 8.5 \times 10^6$ cm Hz$^{1/2}$ W^{-1} at 300 K. This novel device demonstrates a significant improvement in terms of temperature of operation (300 K), possibly making it the first room temperature semiconductor IR detector.

(a)

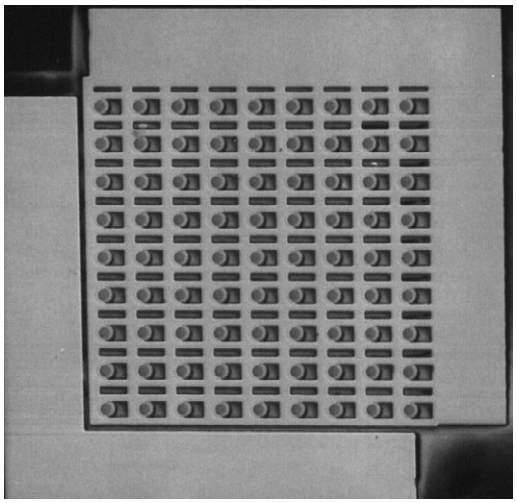

(b)

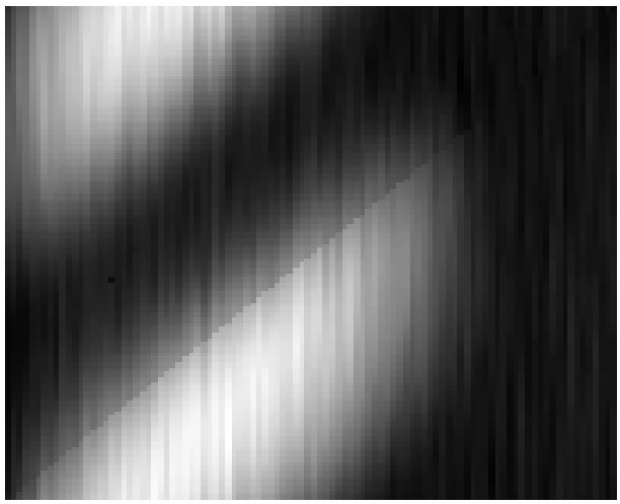

Figure 7. (*a*) SEM micrograph of a (9 × 9) interconnected, non-addressable InAs/GaAs QDIP array with 40 μm mesa size and 120 μm pitch; (*b*) Raster-scanned image obtained from the (13 × 13) QDIP array at 80 K of a 500°C heating element from a hot plate, showing two metal strips.

4. Raster-scan imaging using QDIP array

The photomicrograph of an interconnected (9 × 9) QDIP array is shown in figure 7(*a*). The entire array has a single top contact and a single bottom contact for all of the pixels, effectively behaving as a single detector with a very large optical area and generating a single photocurrent signal. So, the average photocurrent from the array should be large, and therefore much easier to distinguish from the background noise. Our measurements indicated that the dark current is fairly uniform (for 0.1 V bias, the standard deviation, σ, is 3.07×10^{-5}) across this small array despite the large inhomogeneity that is characteristic of the self-organized growth mode. However, it is obvious that FPAs will involve larger areas on the grown wafer.

Raster scanning of the field-of-view (object to be imaged or infrared source) was accomplished using two gold-plated mirrors (highly-reflective in the MWIR and LWIR ranges) servo-actuated by galvanometers and mounted

in an XY bracket. User interfacing with the galvanometers' drive circuitry is achieved with a computer-interfaced scan controller. The raster scan motion of the mirrors directs the infrared light onto the QDIP for detection. The (13×13) QDIP array, with which the imaging experiments were conducted, was housed in a cryostat with a KRS-5 entrance window and held at a temperature of 80 K. The photocurrent produced in the QDIP array is amplified by a low-noise current amplifier, which also provides the bias to the array. The output is further amplified by lock-in techniques, and the amplified signal is transmitted to the data acquisition system wherein each photocurrent/voltage signal obtained from the QDIP corresponds to the raster scan mirror positions and hence to a segment of the field-of-view. Figure 7(*b*) depicts the partial image, limited by the field-of-view of the scanning mirrors, of the heating element of a hot plate at 500°C. Portions of the heated strips are seen as the bright regions. The width of each metal strip is 2 cm with a 1.5 cm space between strips. Fabrication and testing of FPAs made with QDIPs are in progress.

5. Conclusion

It is evident that by increasing the QD absorption volume in QDIPs as well as by separating the dark- and photocurrents, the detector responsivity, conversion efficiency and specific detectivity can be improved and the devices can operate at higher temperatures. We have presented the characteristics of MWIR QDIP with three types of heterostructure design in the active region. In a 70-dot layer QDIP, we demonstrate a responsivity of $0.12\,\mathrm{A\,W^{-1}}$ at an operating temperature of 175 K. In the SL DWELL QDIP, taking advantage of the increased QD density, we have measured an extremely high responsivity ($2.5\,\mathrm{A\,W^{-1}}$) and high conversion efficiency (70%) at a temperature of 78 K. In a resonant T-QDIP, the peak responsivity is $0.75\,\mathrm{A\,W^{-1}}$ at 80 K for a bias of -2 V and the specific detectivity D^* is $2.4 \times 10^{10}\,\mathrm{cm\,Hz^{1/2}\,W^{-1}}$ at the same temperature and applied bias. This detector is also sensitive to 17 μm radiation with $D^* = 8.5 \times 10^6\,\mathrm{cm\,Hz^{1/2}\,W^{-1}}$. Through the use of a raster-scan imaging system, we have been able to demonstrate infrared imaging with QDIP arrays.

Acknowledgments

The work at the University of Michigan is supported by the Army Research Office (MURI programme) under Grant DAAD19-01-1-0462 and the Georgia State University by the National Science Foundation under Grant ECS-0140434. The authors are grateful to S W Kennerly from the Army Research Laboratory, Adelphi, MD and S Gunapala, S Bandara and S B Rafol from the Jet Propulsion Laboratory, Pasadena, CA for their help in measurements.

References

[1] Phillips J, Kamath K and Bhattacharya P 1998 *Appl. Phys. Lett.* **72** 2020
[2] Maimon S, Finkman E and Bahir G 1998 *Appl. Phys. Lett.* **73** 2003
[3] Pan D, Towe E and Kennerly S 1998 *Appl. Phys. Lett.* **73** 1937
[4] Urayama J, Norris T B, Singh J and Bhattacharya P 2001 *Phys. Rev. Lett.* **86** 4930
[5] Kochman B, Stiff-Roberts A D, Chakrabarti S, Phillips J D, Krishna S, Singh J and Bhattacharya P 2003 *IEEE J. Quantum Electron.* **39** 459
[6] Kim E, Madhukar A, Ye A and Campbell J C 2004 *Appl. Phys. Lett.* **84** 3277
[7] Stiff A D, Krishna S, Bhattacharya P and Kennerly S 2001 *IEEE J. Quantum Electron.* **37** 1412
[8] Pierz K, Miglo A, Hinze P, Ahlers F J, Ade G, Hapke-Wurst I, Zeitler U and Haug R J 2001 *Phys. Status Solidi b* **224** 119
[9] Jiang L, Li S S, Yeh N T, Chyi J I, Ross C E and Jones K S 2003 *Appl. Phys. Lett.* **82** 1986
[10] Krishna S, Raghavan S, von Winckel G, Stintz A, Ariyawansa G, Matsik S G and Perera A G U 2003 *Appl. Phys. Lett.* **83** 2745
[11] Raghavan S, Rotella P, Stintz A, Fuchs B, Krishna S, Morath C, Cardimona D A and Kennerly S W 2002 *Appl. Phys. Lett.* **81** 1369
[12] Su X H, Chakrabarti S, Stiff-Roberts A D and Bhattacharya P 2004 *Electron. Lett.* **40** 1082